Hindawi Publishing Corporation
Journal of Nanoparticles
Volume 2016, Article ID 8037013, 7 pages
http://dx.doi.org/10.1155/2016/8037013

Research Article

Synthesis, Characterization, and Photocatalytic Performance of Mesoporous α-Mn_2O_3 Microspheres Prepared via a Precipitation Route

Manoj Pudukudy and Zahira Yaakob

Department of Chemical and Process Engineering, Faculty of Engineering and Built Environment, Universiti Kebangsaan Malaysia, 43600 Bangi, Selangor, Malaysia

Correspondence should be addressed to Manoj Pudukudy; manojpudukudy@gmail.com

Received 23 October 2015; Revised 19 January 2016; Accepted 26 January 2016

Academic Editor: Raphael Schneider

α-Mn_2O_3 microspheres with high phase purity, crystallinity, and surface area were synthesized by the thermal decomposition of precipitated $MnCO_3$ microspheres without the use of any structure directing agents and tedious reaction conditions. The prepared Mn_2O_3 microspheres were characterized by Fourier transform infrared (FTIR) spectroscopy, powder X-ray diffraction (XRD), scanning electron microscopy (SEM), energy-dispersive X-ray spectroscopy (EDS), transmission electron microscopy (TEM), and Brunauer-Emmett-Teller (BET) and photoluminescence (PL) studies. The complete thermal transformation of $MnCO_3$ to Mn_2O_3 was clearly shown by the FTIR and XRD analysis. The electron microscopic images clearly confirmed the microsphere-like morphology of the products with some structural deformation for the calcined Mn_2O_3 sample. The mesoporous texture generated from the interaggregation of subnanoparticles in the microstructures is visibly evident from the TEM and BET studies. Moreover, the Mn_2O_3 microstructures showed a moderate photocatalytic activity for the degradation of methylene blue dye pollutant under UV light irradiation, using air as the potential oxidizing agent.

1. Introduction

The semiconductor based photocatalysis is a promising technique for the abatement of environmental pollutants, especially for the waste water treatment. It has received a significant attention due to its advantages over the traditional methods, especially for the rapid oxidation of pollutants without any polycyclic product formation [1]. In recent years, manganese oxide nano/micromaterials have attracted more attention based on its enhanced semiconductor properties [2]. Among the various crystalline phases of manganese oxides, such as MnO, MnO_2, Mn_2O_3, and Mn_3O_4, the manganese sesquioxide, Mn_2O_3, is of potential interest [3]. It has found promising application in rechargeable batteries, magnetic sensors, super capacitors, and so on [4–7]. Based on this fact, more research is ongoing in its synthesis and characterization. Numerous methods have been developed for the synthesis of phase pure Mn_2O_3 crystals with various attractive morphologies such as wires, rods, spheres, cubes, and hollow and octahedral structures and high porosity [8, 9]. Sol gel, precipitation, hydrothermal, solvothermal, and so forth are the main methods employed for its synthesis [10]. However, many of the aforesaid methods use tough reaction conditions and structure directing agents for the development of a particular morphology and also for the porosity [11]. Therefore, it is quite important to synthesize the phase pure Mn_2O_3 with high porosity/surface area by a facile method without the use of any templates and harsh reaction conditions.

Previously we had reported the synthesis and characterization of mesoporous Mn_2O_3 microspheres by the thermal decomposition of hydrothermally treated $MnCO_3$ microspheres [11]. Herein, we report a facile precipitation method for the synthesis of porous Mn_2O_3 microspheres. Moreover, in the present work, the catalytic performance of the Mn_2O_3

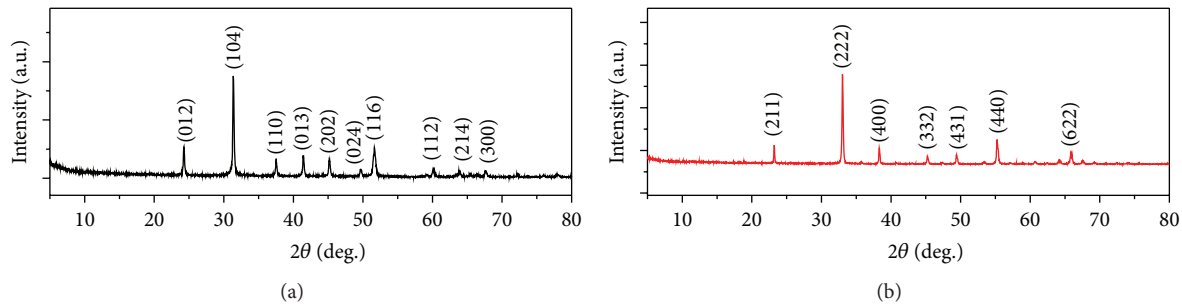

Figure 1: XRD patterns of the (a) precipitated and (b) calcined sample.

powder was studied using methylene blue degradation under UV light irradiation using air as the potential oxidizing agent.

2. Experimental

2.1. Synthesis of Mn_2O_3 Microstructures. All the chemicals used in this study were of analytical grade and were used without further purification. In the typical synthesis, 0.1 mol $MnSO_4{\cdot}4H_2O$ (Sigma Aldrich) and ammonium carbonate (R&M chemicals) were dissolved in 500 mL distilled water separately. Then the ammonium carbonate solution was dropwise added to the Mn solution with magnetic stirring. The precipitates derived from the reaction between these two solutions were collected, washed with distilled water, and dried at 100°C overnight. Finally the precipitated intermediate precursor was calcined at 600°C for 5 h to obtain the final product.

2.2. Characterization of Materials. The prepared powder samples were characterized by powder X-ray diffraction (XRD, Bruker D8 Advance diffractometer), Fourier transform infrared spectroscopy (FTIR, Thermo Scientific NICOLET 6700), field emission scanning electron microscopy (FESEM, Zeiss SUPRA 55) equipped with an energy-dispersive X-ray (EDX) spectroscope, transmission electron microscopy (TEM, Phillips CM-12, operated at an accelerating voltage of 100 kV), and Brunauer-Emmett-Teller and Barrett-Joyner-Halenda (BET/BJH, Micromeritics ASAP 2010) analysis. The optical characterization was performed using a photoluminescence spectroscopy (PL, FLSP920 Edinburgh, $\lambda = 257$ nm).

2.3. Photocatalytic Experiments. The catalytic performance of the Mn_2O_3 sample was studied using the photodegradation of methylene blue (MB) under UV light irradiation. In this procedure, 50 mg catalyst was suspended in 50 mL MB solution (2.5 mg/L) and stirred for 30 minutes in dark, to ensure the accomplishment of adsorption-desorption equilibrium. Then the solution was placed in a Rayonet-type photoreactor (Associate Technical, India) with 16 UV lamps (HITACHI, F8T5 8 WATT Hitachi, Ltd., Tokyo, Japan, made in Japan, radiation wavelength of 352 nm) and aerated. At particular time interval, the solution was withdrawn and centrifuged and its absorbance (λ at 664 nm) was measured for the calculation of degradation percentage using a UV-vis spectrophotometer (Varian Cary, Perkin Elmer Lambda-35). The removal efficiency was calculated by the function of $((A_0 - A_t)/A_0) \times 100\%$, where A_0 is the initial absorbance of MB and A_t is the absorbance left after the reaction, at the time "t."

3. Results and Discussion

3.1. Materials Characterization. Figure 1(a) shows the XRD patterns of the precipitated intermediate precursor. The diffraction peaks at the 2θ values of 24.2°, 31.2°, 37.5°, 41.4°, 45.1°, 51.4°, 51.7°, 60°, 64.2°, 68.2°, and 78° can be directly indexed to the rhombohedral crystalline structure of $MnCO_3$ with the lattice parameters $a = b = 0.4790$ nm and $c = 1.569$ nm (JCPDS: 00-044-1472). No other peaks were identified, indicating the phase purity of the precipitated $MnCO_3$. Figure 1(b) shows XRD pattern of the sample calcined at 600°C. The diffraction peaks at the 2θ values, whose (hkl) planes are marked, correspond to the body centered cubic phase crystalline structure of Bixbyite-C syn Mn_2O_3 with the lattice parameter $a = 0.9409$ nm (JCPDS: 00-041-1442). No impure peaks related to other phases were noticed, indicating the high phase purity of the product.

Elemental composition of the samples was confirmed by the EDX analysis as shown in Figure 2. Figure 2(a) shows the EDX spectra of $MnCO_3$ with the main peaks of Mn, C, and O as elements. The manganese oxide was also found to be highly pure, because the results specify that the calcined sample has only Mn and O as elements without any other elemental impurities. The atomic ratio of Mn to O was found to be 39 : 61, which is the same as in the stoichiometric ratio of Mn_2O_3 [12].

Figure 3(a) shows the FTIR spectrum of the intermediate precursor. It shows a strong well resolved band at ~1388 cm^{-1} due to the fingerprint stretching vibration of the carbonate species. The other bands at ~721 cm^{-1} and ~861 cm^{-1} were related to the planar vibrations of the carbonate units [13]. These observations further confirm the formation of $MnCO_3$. FTIR spectrum of the product is shown in Figure 3(b). It is clear that the bands of carbonate units were completely removed after calcination, indicating the thermal decomposition of $MnCO_3$ with the release of carbonate groups. The more or less resolved transmission bands located

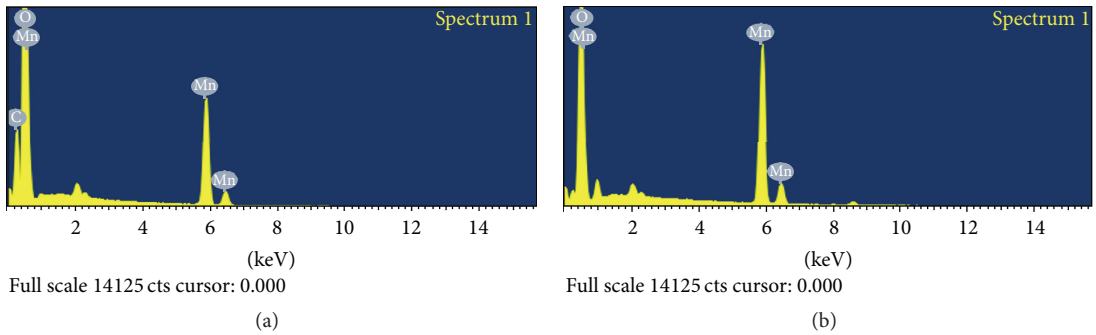

Figure 2: EDX spectra of the (a) precipitated and (b) calcined product.

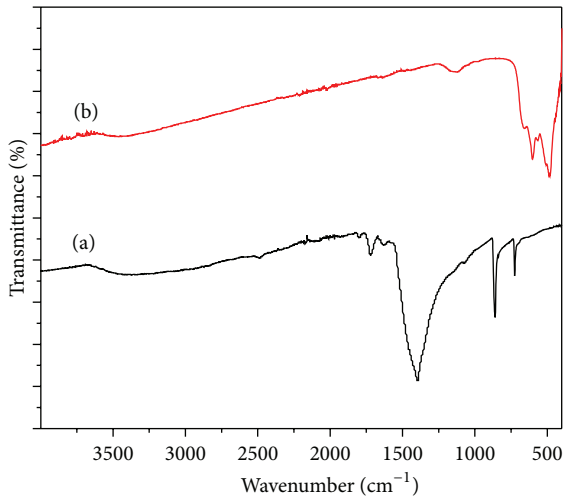

Figure 3: FTIR spectra of the (a) precipitated and (b) calcined product.

at ~481 cm^{-1}, ~611 cm^{-1}, and ~668 cm^{-1} were attributed to the formation of manganese oxides. The bands at 667 cm^{-1} and 611 cm^{-1} were attributed to the asymmetric and symmetric stretching vibration of Mn–O–Mn bond in transmission mode [14]. The resolved sharp band located at around 481 cm^{-1} has arisen due to the bending vibration of the Mn–O bond [15]. A weak broad band at ~3500 cm^{-1} was assigned to the stretching vibration of the O–H group, due to the absorbed water molecules.

Morphology of the samples was examined by FESEM and the images at different magnifications were taken. The sphere-like morphology of $MnCO_3$ with the average size of 2–4 micrometres is shown in Figure 4. Along with the microspheres, some microcubes were also observed. The surface of the microspheres was found to be fine, smooth, and nonporous and has comb tips. The tendency of the $MnCO_3$ nuclei to attain the most stable thermodynamic state with minimal surface energy is responsible for the formation of spherical shape [16]. The SEM images of the calcined product are shown in Figure 5. It shows the porous spherical morphology of the Mn_2O_3 microstructures. Moreover, some structural deformation was observed. Here, the morphology is not much preserved as compared to our previously reported sample [11]. However, the conserved morphology indicates the self-sacrificing template character of the precipitated $MnCO_3$. Moreover, the release of a large amount of CO_x from the bulk of sample developed pores in the sample. The high magnified image shown in Figure 5(d) shows the manganese oxide subnanoparticles, which are more or less spherical, elongated, and interaggregated to gain a porous structure. The TEM images shown in Figure 6 confirm this observation.

The textural properties of the calcined product were studied using BET/BJH analysis. The N_2 sorption isotherm of the Mn_2O_3 microspheres is shown in Figure 7. The sample displayed a type IV isotherm, with H3 hysteresis loop, indicating the presence of a well-organized mesoporous texture in the sample. The mesoporosity is aroused from interaggregation of the subnanoparticles as shown in the TEM images. The specific surface area calculated by the BET method was found to be 32 m^2/g with a mean pore size of 18 nm and a cumulative pore volume of 0.0936 cm^3/g.

The optical properties of the Mn_2O_3 microstructures were investigated by room temperature PL spectroscopy. The PL spectrum of the Mn_2O_3 microspheres is shown in Figure 8. It shows an intense emission band in the UV region, at ~390 nm. This band is attributed to the recombination of electrons and holes in the conduction and valence band, respectively, that is, the annihilation of excitons [17, 18]. The high intensity of the UV band indicates its crystalline quality and applications under UV light [19].

3.2. Photocatalytic Activity of Mn_2O_3 Microspheres. Mesoporous semiconductors with high surface area have a great role in photocatalysis [20]. To validate the catalytic performance of the Mn_2O_3 microspheres, photodegradation of methylene blue was investigated under UV light irradiation. The photocatalytic activity of Mn_2O_3 was rarely reported, even though Mn_2O_3 shows usual semiconductor properties. It was hardly used as a good photocatalyst, although it has been widely applied in electrochemical field. The photocatalytic efficiency was found to be too low compared to the common semiconductor photocatalysts such as TiO_2,

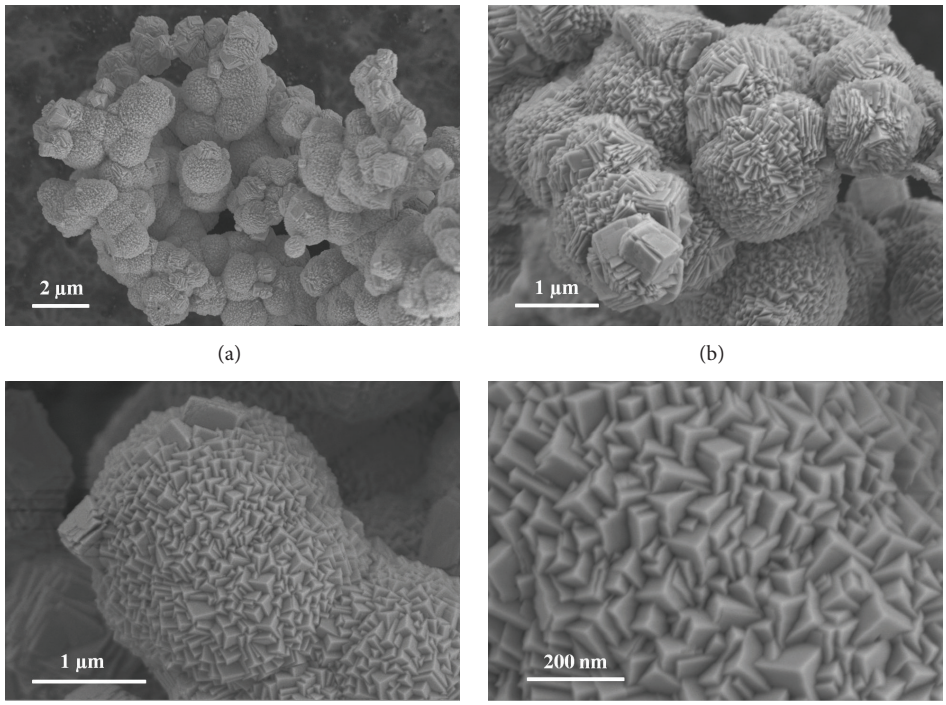

(a) (b)

(c) (d)

Figure 4: FESEM photographs of the intermediate precursor $MnCO_3$.

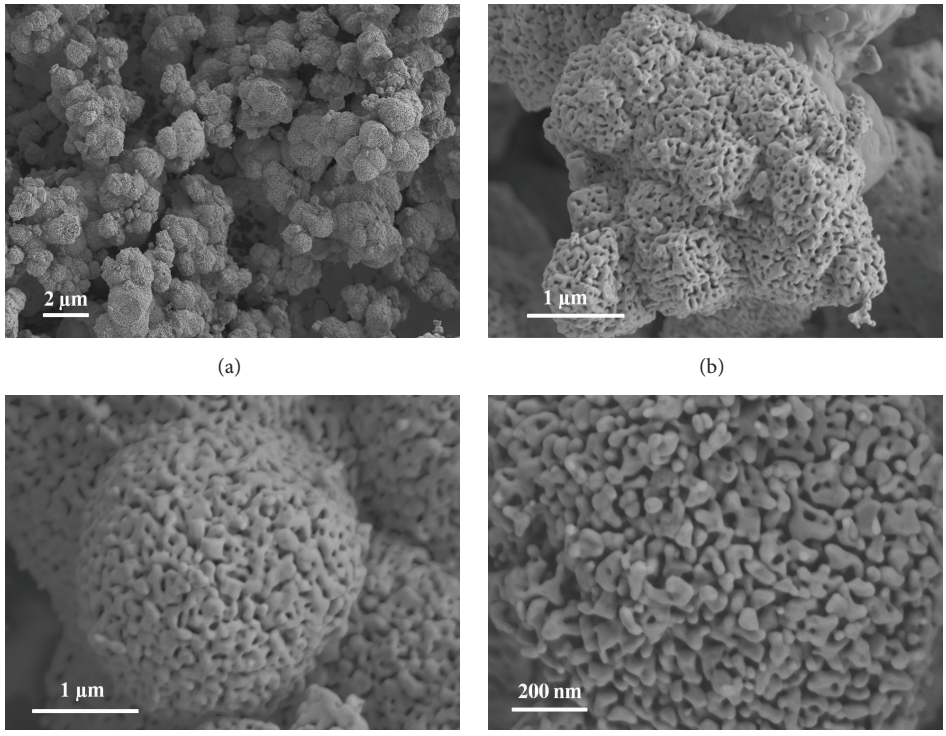

(a) (b)

(c) (d)

Figure 5: FESEM photographs of the Mn_2O_3 microstructures.

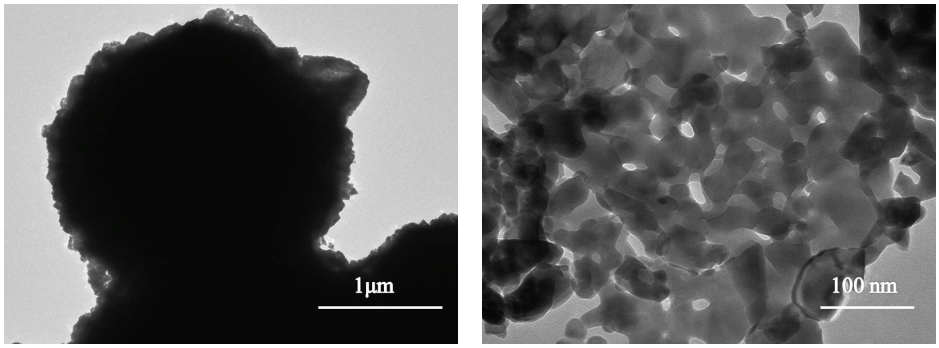

Figure 6: TEM images of the calcined Mn_2O_3 product.

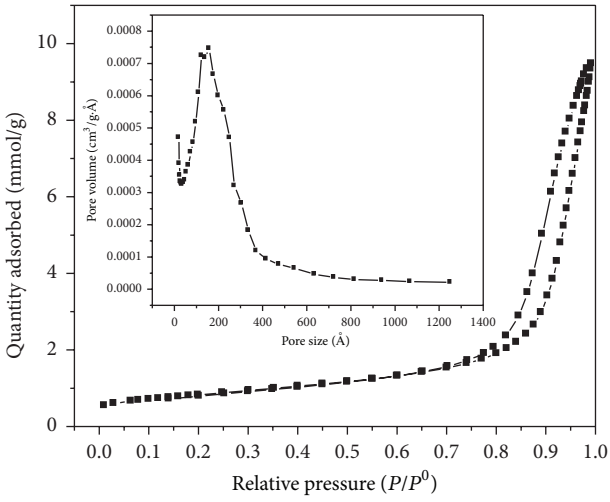

Figure 7: BET/BJH plots of the Mn_2O_3 microspheres.

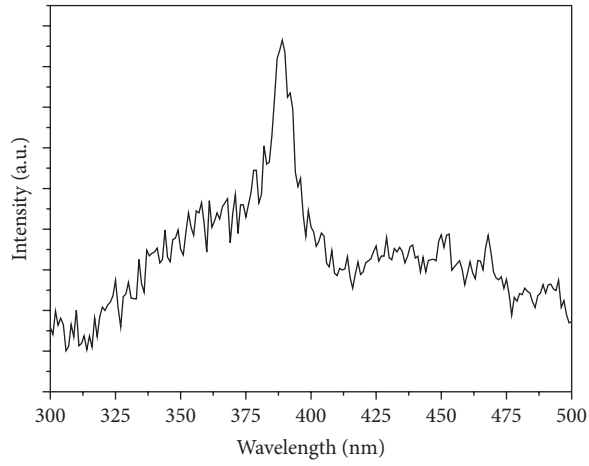

Figure 8: PL spectrum of the Mn_2O_3 microspheres.

ZnO and other photoactive materials. Previously Gnanam and Rajendran [19] reported the photocatalytic degradation of Remazol Red B over Mn_2O_3 nanodumbbells synthesized by a hydrothermal method using several ionic surfactants. As per their report, a maximum degradation efficiency of 71% was observed for the manganese oxide sample prepared using sodium dodecyl sulfate (SDS) as the anionic surfactant. Herein, we studied the photocatalytic activity of Mn_2O_3 microspheres for the degradation of methylene blue for the first time. Under UV light irradiation, 6% self-degradation of methylene blue was observed (Figure 9(a)). Also there is no significant change in the absorbance of dye solution, when the reaction was conducted in dark/adsorption condition (~2%). But the addition of porous Mn_2O_3 microspheres increased the photodegradation rate to a considerable extent and 32% degradation was achieved within 5 h (Figure 9(c)). The decrease in the absorbance of the dye solution shown in Figure 9(d) depicts the lowering of dye concentration by the destruction of dye molecules [21]. The degradation further increased to 38% at 6 h reaction, which indicates that the rate of degradation linearly increases with reaction time. The obtained results confirm that our samples also have a considerable catalytic activity for the photocatalytic dye degradation and demonstrated its applicability for the waste water treatment. Moreover, it showed higher activity than commercial MnO powder as shown in Figure 9(b).

4. Conclusions

In summary, α-Mn_2O_3 microspheres were successfully synthesized by the thermal decomposition of precipitated $MnCO_3$ microspheres. The complete thermal transformation of $MnCO_3$ to Mn_2O_3 was observed by the FTIR and XRD results. The use of any structure directing agents and harsh reaction conditions were excluded during the preparation of the samples. The formation of body centered cubic phase crystalline structure of Mn_2O_3 without any other impure phases was confirmed by the powder XRD analysis. The electron microscopy analyses showed the microsphere-like morphology of the intermediate precursor and the calcined products. Some structural deformation was observed for the calcined Mn_2O_3 sample. The mesoporosity generated from the interaggregation of the subnanoparticles was confirmed by TEM images. The specific surface area measured by the BET method was found to be 32 m^2/g with a monomodal

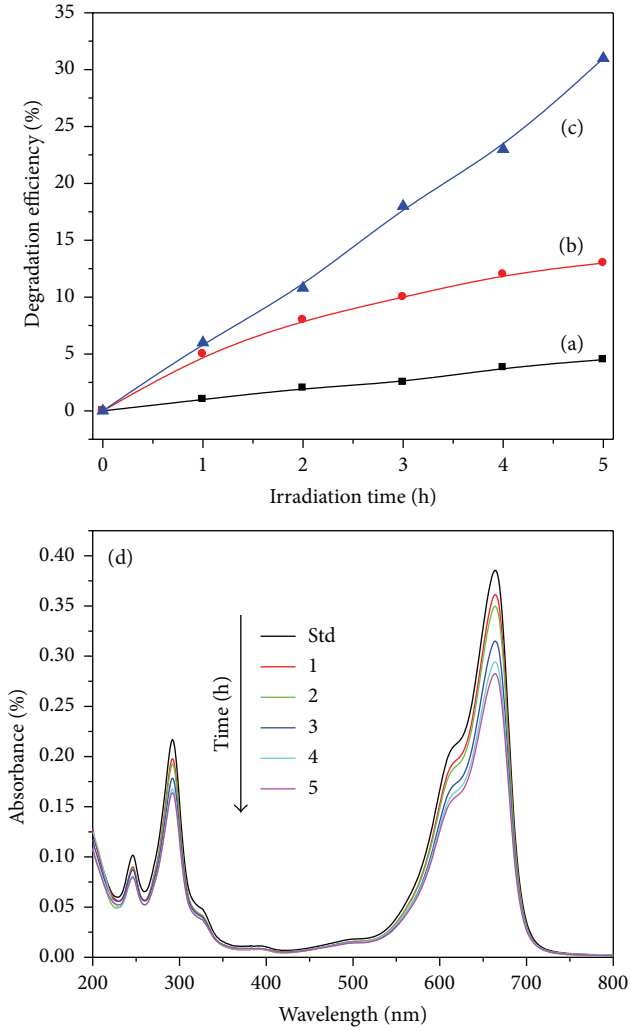

FIGURE 9: Efficiency of the Mn_2O_3 microspheres for MB degradation (50 mL 2.5 mg/L MB solution, 0.05 g catalyst, constant air bubbling, and UV irradiation). (a) Without Mn_2O_3, (b) commercial MnO, (c) Mn_2O_3 microstructures, and (d) changes in the UV absorption spectra of MB solution with time.

mesoporous texture. The Mn_2O_3 microspheres showed a moderate photocatalytic activity (38%) for the degradation of methylene blue dye pollutant over a low catalyst dose (0.05 g) using air as the oxidizing agent.

Conflict of Interests

The authors declare that there is no conflict of interests regarding the publication of this paper.

References

[1] A. D. Paola, E. G. López, G. Marcì, and L. Palmisano, "A survey of photocatalytic materials for environmental remediation," *Journal of Hazardous Materials*, vol. 211-212, pp. 3–29, 2012.

[2] P. Su, D. Chu, and L. Wang, "Studies on catalytic activity of nanostructure Mn_2O_3 prepared by solvent-thermal method on degrading crystal violet," *Modern Applied Science*, vol. 4, no. 5, pp. 125–129, 2010.

[3] Z. Yang, W. Zhang, Q. Wang, X. Song, and Y. Qian, "Synthesis of porous and hollow microspheres of nanocrystalline Mn_2O_3," *Chemical Physics Letters*, vol. 418, no. 1–3, pp. 46–49, 2006.

[4] H.-G. Jung, M. W. Jang, J. Hassoun, Y.-K. Sun, and B. Scrosati, "A high-rate long-life $Li_4Ti_5O_{12}/Li[Ni_{0.45}Co_{0.1}Mn_{1.45}]O_4$ lithium-ion battery," *Nature Communications*, vol. 2, pp. 516–520, 2011.

[5] X. Chen, X. Li, Y. Jiang, C. Shi, and X. Li, "Rational synthesis of α-MnO_2 and γ-Mn_2O_3 nanowires with the electrochemical characterization of α-MnO_2 nanowires for supercapacitor," *Solid State Communications*, vol. 136, no. 2, pp. 94–96, 2005.

[6] X.-M. Liu, S.-Y. Fu, and C.-J. Huang, "Synthesis, characterization and magnetic properties of β-MnO_2 nanorods," *Powder Technology*, vol. 154, no. 2-3, pp. 120–124, 2005.

[7] S. Thota, B. Prasad, and J. Kumar, "Formation and magnetic behaviour of manganese oxide nanoparticles," *Materials Science and Engineering: B*, vol. 167, no. 3, pp. 153–160, 2010.

[8] N. Chandra, S. Bhasin, M. Sharma, and D. Pal, "A room temperature process for making Mn_2O_3 nano-particles and γ-MnOOH nano-rods," *Materials Letters*, vol. 61, no. 17, pp. 3728–3732, 2007.

[9] J. Cao, Q. Mao, and Y. Qian, "Synthesis of Mn_2O_3 homogeneous core/hollow-shell structures with excellent adsorption performance," *Journal of Solid State Chemistry*, vol. 191, pp. 10–14, 2012.

[10] F. Davar, F. Mohandes, and M. Salavati-Niasari, "Synthesis and characterization manganese oxide nanobundles from decomposition of manganese oxalate," *Inorganica Chimica Acta*, vol. 362, no. 10, pp. 3663–3668, 2009.

[11] M. Pudukudy, Z. Yaakob, and R. Rajendran, "Facile synthesis of mesoporous α-Mn_2O_3 microspheres via morphology conserved thermal decomposition of $MnCO_3$ microspheres," *Materials Letters*, vol. 136, pp. 85–89, 2014.

[12] W. He, Y. Zhang, X. Zhang, H. Wang, and H. Yan, "Low temperature preparation of nanocrystalline Mn_2O_3 via ethanol-thermal reduction of MnO_2," *Journal of Crystal Growth*, vol. 252, no. 1-3, pp. 285–288, 2003.

[13] H. Hu, J.-Y. Xu, H. Yang, J. Liang, S. Yang, and H. Wu, "Morphology-controlled hydrothermal synthesis of $MnCO_3$ hierarchical superstructures with Schiff base as stabilizer," *Materials Research Bulletin*, vol. 46, no. 11, pp. 1908–1915, 2011.

[14] M. Salavati-Niasari, F. Mohandes, F. Davar, and K. Saberyan, "Fabrication of chain-like Mn_2O_3 nanostructures via thermal decomposition of manganese phthalate coordination polymers," *Applied Surface Science*, vol. 256, no. 5, pp. 1476–1480, 2009.

[15] S. M. Pourmortazavi, M. Rahimi-Nasrabadi, A. A. Davoudi-Dehaghani, A. Javidan, M. M. Zahedi, and S. S. Hajimirsadeghi, "Statistical optimization of experimental parameters for synthesis of manganese carbonate and manganese oxide nanoparticles," *Materials Research Bulletin*, vol. 47, no. 4, pp. 1045–1050, 2012.

[16] S. Lei, X. Peng, X. Li et al., "Novel detached system to $MnCO_3$ nanowires: a self-sacrificing template for homomorphous Mn_3O_4 and α-Mn_2O_3 nanostructures," *Materials Chemistry and Physics*, vol. 125, no. 3, pp. 405–410, 2011.

[17] M. Pudukudy and Z. Yaakob, "Hydrothermal synthesis of mesostructured ZnO micropyramids with enhanced photocatalytic performance," *Superlattices and Microstructures*, vol. 63, pp. 47–57, 2013.

[18] J. Q. Hu and Y. Bando, "Growth and optical properties of single crystal tubular ZnO whiskers," *Applied Physics Letters*, vol. 82, no. 9, pp. 1401–1403, 2003.

[19] S. Gnanam and V. Rajendran, "Facile hydrothermal synthesis of alpha manganese sesquioxide (α-Mn_2O_3) nanodumb-bells: structural, magnetic, optical and photocatalytic properties," *Journal of Alloys & Compounds*, vol. 550, pp. 463–470, 2013.

[20] Y. Chen, L. Hu, M. Wang, Y. Min, and Y. Zhang, "Self-assembled Co_3O_4 porous nanostructures and their photocatalytic activity," *Colloids and Surfaces A: Physicochemical and Engineering Aspects*, vol. 336, no. 1–3, pp. 64–68, 2009.

[21] M. Pudukudy and Z. Yaakob, "Facile solid state synthesis of ZnO hexagonal nanogranules with excellent photocatalytic activity," *Applied Surface Science*, vol. 292, pp. 520–530, 2014.